

Intercomparison and Evaluation of Cumulus Parameterizations Under Summertime Mid-Latitude Continental Conditions

*S. C. Xie, R. T. Cederwall, and J. J. Yio
Lawrence Livermore National Laboratory
Livermore, California*

*K.-M. Xu
National Aeronautics and Space Administration
Langley Research Center
Hampton, Virginia*

Introduction

Parameterization of cumulus convection in general circulation models (GCMs) is recognized as one of the most important and complex issues in model physical parameterizations. In earlier studies, most cumulus parameterizations were developed and evaluated using data observed over tropical oceans, such as the Global Atmospheric Research Program's Atlantic Tropical Experiment (GATE) data. This is partly due to inadequate field measurements in the mid-latitudes. In this study, we compare and evaluate a total of eight types of state-of-the-art cumulus parameterizations used in fifteen single-column models (SCMs) under summertime mid-latitude continental conditions using the Atmospheric Radiation Measurement (ARM) Program Southern Great Plains (SGP) summer 1997 intensive operational period (IOP) data, which covers several continental convection events. Our purpose is to systematically compare and evaluate the performance of these cumulus parameterizations under summertime mid-latitude continental conditions. Through the study we hope to identify strengths and weaknesses of these cumulus parameterizations that will lead to further improvements. Here, we briefly present our most interesting results. A full description of this study can be seen in Xie et al. (2001).

Model Descriptions

Table 1 lists the 15 SCMs that participated in the intercomparison study. The deep convection schemes and some relevant aspects of these schemes are listed in Table 2. In Table 2, AS represents the scheme proposed by Awakawa and Schubert (1974) and ZM represents the scheme proposed by Zhang and McFarlane (1995). As shown, all of the deep convection schemes are based on the mass flux approach, which uses either spectral cloud ensemble models similar to AS (i.e., CSU, GFDL, and McRAS) or a bulk cloud ensemble model (i.e., CSIRO, ECMWF, GISS, MesoNH, PNNL/CCM2, and MOUM). In a bulk cloud ensemble model, only one single cloud model is used to represent an average overall cloud type within a convective ensemble. The ZM type of schemes used in CCCma0, CCCma1/SP, CCM3, CCM3/SIO, CCM3/SUNY, and Scripps is different from the conventional bulk

Model (SCM)	Model Full Name
CCCma0	Canadian Center for Climate Modeling and Analysis, Version 0
CCCma1/SP	Canadian Center for Climate Modeling and Analysis, Version 1
CCM3	NCAR Community Climate Model, Version 3
CCM3/SIO	Scripps Institution of Oceanography Version of CCM3
CCM3/SUNY	State University of New York at Stony Brook Version of CCM3
CSIRO	Commonwealth Scientific and Industrial Research Organization Mark 3
CSU	Colorado State University GCM
ECMWF	European Center for Medium-range Weather Forecasts
GFDL	National Oceanic and Atmospheric Administration Geophysical Fluid Dynamics Laboratory
GISS	National Aeronautics and Space Administration Goddard Institute for Space Studies
McRAS	Microphysics of cloud/relaxed arakawa-schubert scheme
MesoNH	Modele mesoechelle non-hydrostatique
PNNL/CCM2	Pacific Northwest National laboratory Version of CCM2
Scripps	Scripps Institution of Oceanography
MOUM	Met Office Unified Model

Model	Convection Scheme	Closure	Trigger	Penetrative Convection
CCCma0	Revised ZM (1)	CAPE	CAPE>0 and Buoyancy at LCL > 0.1K	Yes
CCCma1/SP	Prognostic ZM (1)	Prognostic closure	CAPE>0	Yes
CCM3	ZM (1)	CAPE	CAPE > 0	Yes
CCM3/SIO	Revised ZM (1)	CAPE generation rate	CAPE generation rate > 0	Yes
CCM3/SUNY	Revised ZM (1)	CAPE	Positive dynamic CAPE	Yes
CSIRO	Bulk mass Flux (2)	A stability-dependent mass flux	Local parcel buoyancy	Yes
CSU	Prognostic AS (3)	A prognostic closure using the cumulus kinetic energy	Positive CWF	Yes
ECMWF	Bulk Mass Flux (4)	CAPE	Local parcel buoyancy	Yes
GFDL	Relaxed AS (5)	Relax the state toward quasi-equilibrium	Positive CWF	Yes
GISS	Bulk mass flux (6)	Cloud base neutral buoyancy	Local parcel buoyancy	Yes
McRAS	Revised relaxed AS (5)	Same as GFDL	Positive CWF and RH>RH _{crit}	Yes
MesoNH	Bulk Mass Flux (7)	CAPE	CAPE > 0 and vertical motion	Yes
PNNL/CCM2	Bulk Mass Flux (8)	A stability-dependent mass flux	Local parcel buoyancy	No
Scripps	ZM (1)	CAPE	CAPE > 0	Yes
MOUM	Bulk Mass Flux (2)	CAPE	Local parcel buoyancy	Yes

mass flux schemes. It is based on the same spectral rising plume concept as used in AS. However, by assuming a constant spectral distribution in cloud base mass flux, the thermodynamic equations are reduced to the bulk form.

Closure used in most convection schemes is based on the assumption that convective available potential energy (CAPE) is consumed by cumulus convection over a given time scale (CAPE closure). Some of the bulk mass flux schemes use closure based on a stability-dependent mass flux (i.e., CSIRO, GISS, and PNNL/CCM2). Cumulus convection in most SCMs is triggered either by positive local parcel buoyancy or by positive CAPE or cloud work function (CWF). For some models, other requirements need to be met for triggering model convection (e.g., CCCma0, CCM3/SUNY, McRAS, and MesoNH). Convective-scale precipitation-driven downdrafts are parameterized in most of the models except for PNNL/CCM2, CSU, and GFDL. Almost all models treat convection as penetrative convection except for the convection scheme used in PNNL/CCM2. Detailed descriptions of these schemes can be found in Xie et al. (2001).

Data and Experiment Design

The data used to drive and evaluate the SCMs and CRMs were collected at the ARM SGP site during the summer 1997 IOP, from June 18 (2330 Universal Time Coordinates [UTC]) to July 17 (2330 UTC) (Figure 1). The period contained a wide range of summertime weather conditions. Observations at the

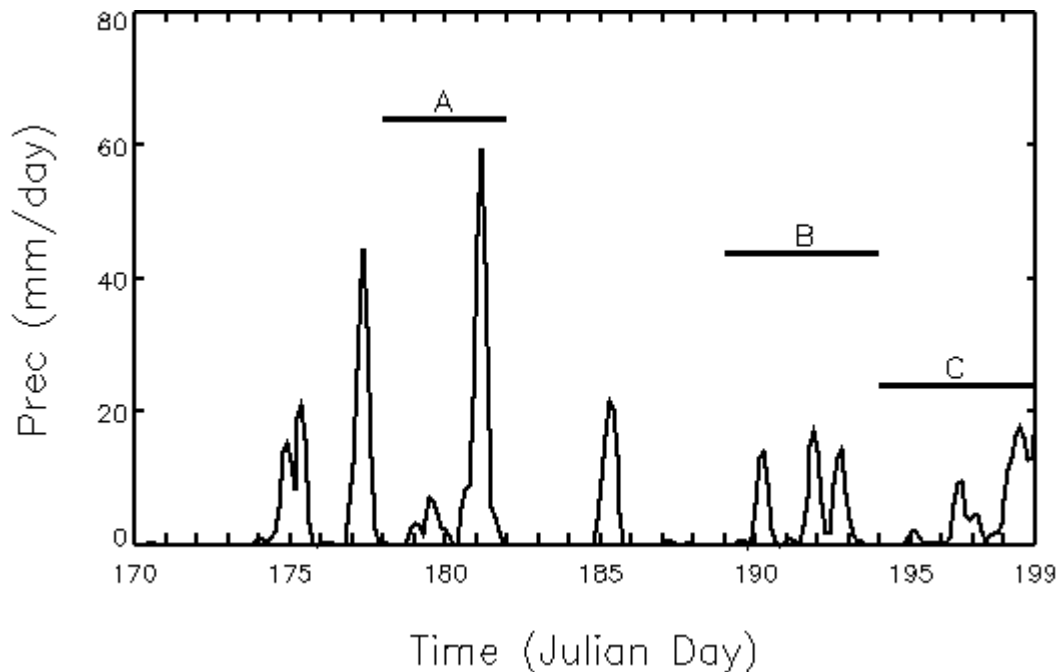


Figure 1. Time series of observed surface precipitation rates (mm/day) during summer 1997 IOP. A, B, and C are the three Subcases selected in the study.

ARM site used in this study to characterize the column include 3 hourly soundings at five locations, surface meteorology network, remote sensing of vertical profiles and integral values, and satellite data; more details are given in Ghan et al. (2000). The horizontal and vertical advective tendencies of temperature and moisture and vertical velocity are derived from the constrained variational analysis (Zhang and Lin 1997; Zhang et al. 2001).

Three precipitating Subcases (A, B, and C), each lasting for 4 or 5 days (Figure 1), are selected to test model performance in this study. For all experiments, the horizontal and vertical advective tendencies of temperature and moisture and surface fluxes are specified from the observations. The radiative heating rates are calculated from model parameterizations. The large-scale forcing for temperature and moisture for the three selected Subcases is shown in Figure 2.

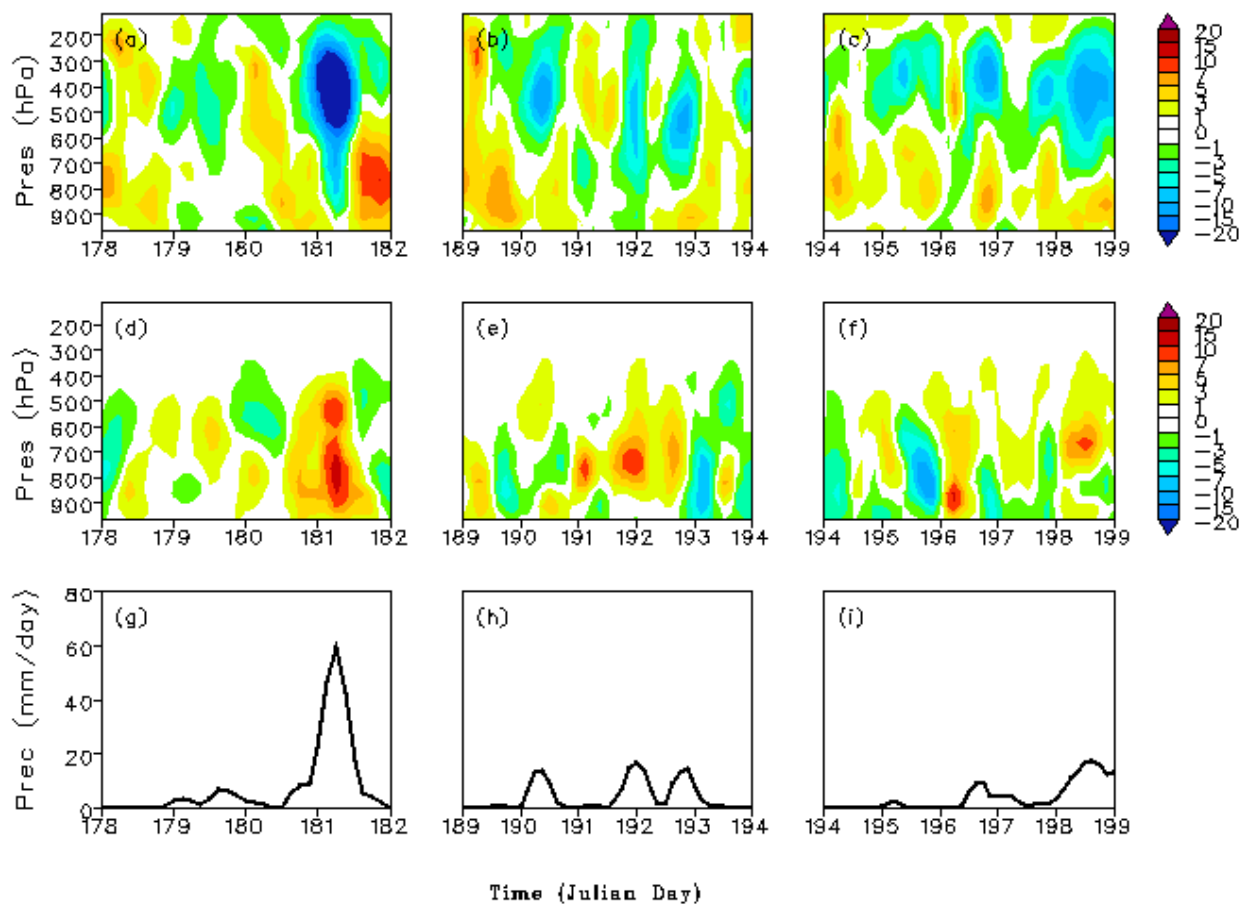


Figure 2. Time-height cross section of observed large-scale advective tendencies of temperature (a - c, K day^{-1}) and moisture (d - e, $\text{g kg}^{-1} \text{day}^{-1}$) and surface precipitation rates (f - h, mm day^{-1}) for Subcases A, B, and C.

Results

Temperature, moisture, and surface precipitation. Figure 3 shows the vertical structures of the temperature and moisture departures from observations, averaged over the three subperiods. For temperature field, it is seen that the intermodel difference is large in the upper and lower troposphere and relatively small in the middle troposphere. In the upper troposphere, models with the ZM and AS types of schemes generally have warm biases and models with the bulk mass flux scheme typically have cold biases there. CCM3 and PNNL/CCM2 are the two typical cases: the former shows the largest warm biases and the latter shows the largest cold biases in the middle and upper troposphere. The cold biases produced in PNNL/CCM2 are related to its non-penetrative convection scheme. More details are seen in Xie et al. (2001). For moisture field, most SCMs show drier atmospheres than the observations at the layers between 500 to 800 hPa. This might be partly related to the neglect of cumulus downdrafts or weak downdrafts produced in the SCMs, as shown later. The simulations are largely diverse below 800 hPa, generally with dry biases in those having warm biases and moist biases in those having cold biases.

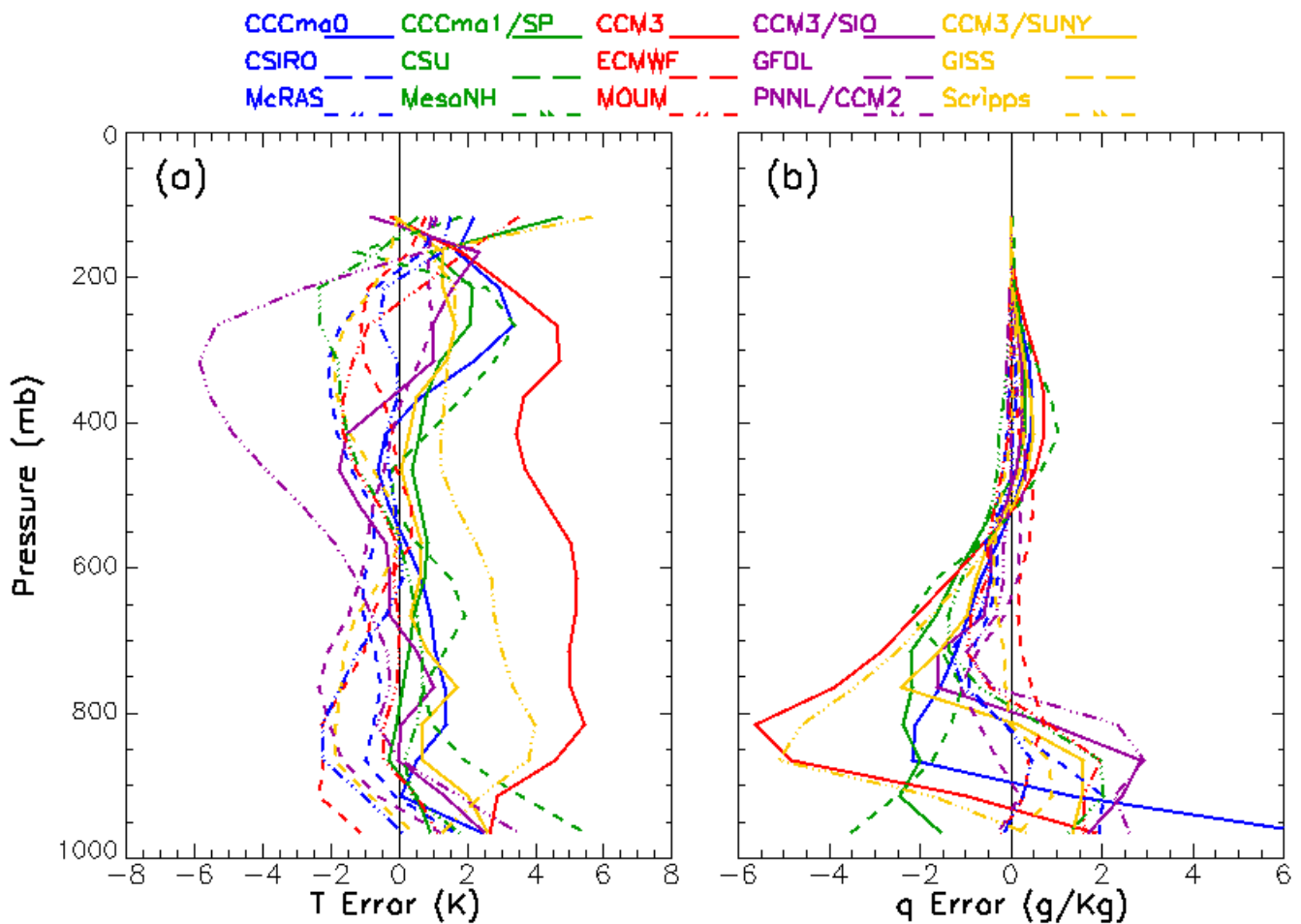


Figure 3. Time-averaged temperature and moisture errors produced by the SCMs over Subcases A, B, and C: (a) temperature error, and (b) moisture error.

Figures 4 (a) and (b) display time-averaged errors of total surface precipitation rate and the temporal correlation coefficients between the model simulated and observed surface precipitation over the three subperiods, respectively. It is seen that the observed precipitation is largely overestimated in those models that have large warm/dry biases (e.g., CCM3 and Scripps) and underestimated in those that produce large cold/moist biases (e.g., PNNL/CCM2). The reason is simply that excessive precipitation is associated with more convective heating released and more moisture consumed, and vice versa.

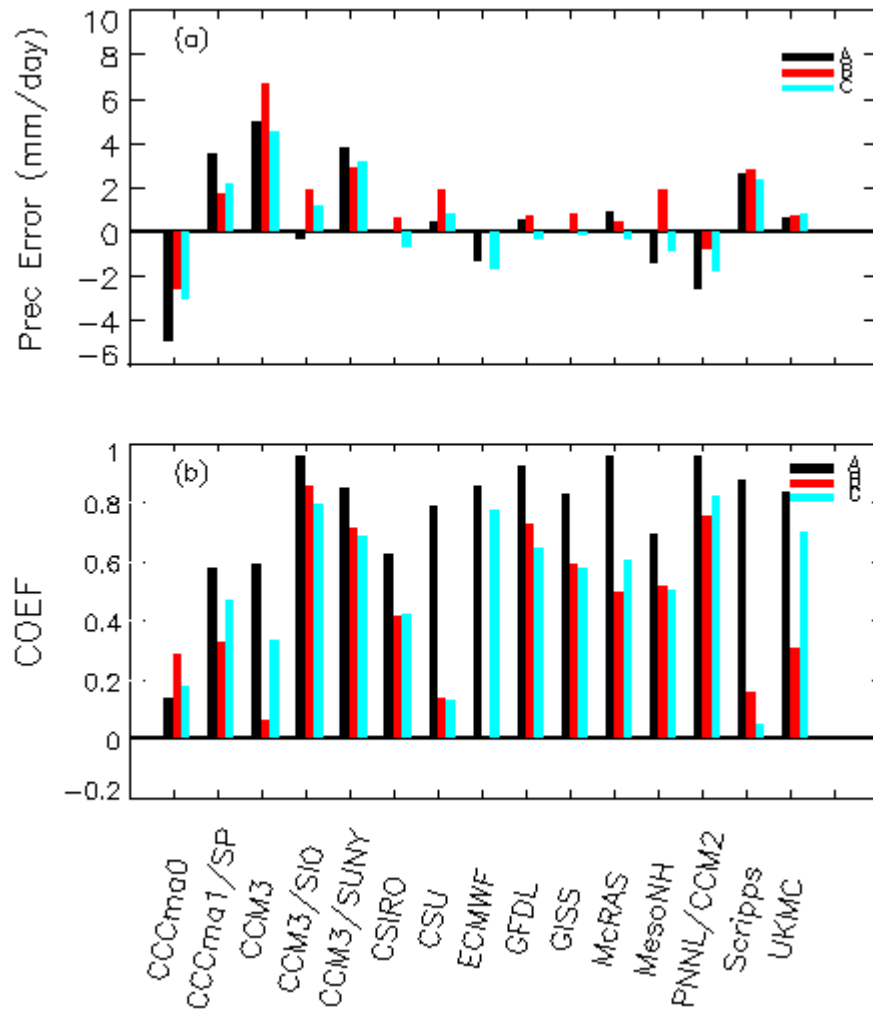


Figure 4. (a) Time-averaged surface precipitation errors produced by the SCMs over Subcases A, B, and C, respectively. (b) Temporal correlation coefficients between observed and simulated surface precipitation rates for Subcases A, B, and C.

It is noted from Figure 4 (b) that all SCMs generally have high correlation coefficients over Subcase A, except for the CCCma0. Recall that Subcase A is characterized by a strong precipitation event associated with strong advective cooling in the middle and upper troposphere and strong advective moistening in the lower troposphere (Figure 2). This infers that most schemes could capture well the convection in such environments. However, the correlation is reduced during Subcases B and C. The

relatively weak large-scale forcing during Subcases B and C, especially the decoupling of the large-scale temperature forcing with the large-scale moisture forcing, as shown in the first precipitation event of Subcase B (Figure 2), is not favorable for generation of model convection. Note that the correlation coefficient is closely associated with the initiation of model convection. It is seen that the correlation is reduced significantly in those models by using positive CAPE and CWF as convective triggering function such as CCM3, CSU, and Scripps. In general, for those that use local parcel buoyancy as the trigger, the correlation is just slightly reduced (e.g., ECMWF and PNNL/CCM2). CCM3/SIO and CCM3/SUNY also show high correlation with the observations during Subcases B and C because of the incorporation of the large-scale dynamic processes in their triggering function.

Problems with the triggering of model convection might be one main reason for the simulation errors because the large-scale advective tendencies of temperature and moisture are specified in SCMs. Because of the lack of efficient internal feedback between the large-scale dynamical processes and physical processes in SCMs, whether model convection is triggered or not could have large impacts on model simulations. The fourth column of Table 2 shows that these convection schemes estimate atmospheric instability either based on the vertical integral of parcel buoyant energy (CAPE) (the AS and ZM types of schemes) or local parcel buoyancy (most bulk mass flux schemes). This could have a potentially large effect on estimating atmospheric instability in an area where the surface latent and sensible heat fluxes and surface radiative fluxes are large, such as over the mid-latitude lands, since the surface processes largely determine the generation and magnitude of CAPE. In fact, thermodynamic structure in the plane boundary layer (PBL) plays an important role in determining the triggering of model convection. Over these areas, the schemes that are based on CAPE could be more active than those based on local parcel buoyancy. As shown in Xie and Zhang (2000), the convection schemes that are only based on positive CAPE to initiate model convection, such as the ZM scheme, can lead to excessive convection in mid-latitude continental regions during daytime since the strong solar diurnal heating largely controls the generation of CAPE.

Cloud Mass Flux

Cumulus mass fluxes are highly related to convective heating/drying profiles; however, they are usually not easy to observe. Thus, in this study, we compare the SCM-produced cumulus mass fluxes with those diagnosed from simulations of CRMs in a companion study (Xu et al. 2001).

Figures 5 (a), (b), and (c), respectively, compare the vertical structure of updraft (M_u), downdraft (M_d), and net (M_c) cloud mass fluxes estimated from the SCMs with those diagnosed from the CRMs averaged over the disturbed periods (observed precipitation rate ≥ 0.36 mm/day) during Subcases A, B, and C. It should be noted that the radiative heating rate is specified from the ECMWF analysis in the CRMs. The black solid line in Figure 5 (c) is the observed large-scale mean mass flux ($M = -\omega$). The black dashed line and small bar represent the mean of the mass fluxes across the ten CRMs and the standard deviations from the mean, respectively. A detailed description of individual CRM results can be found in Xu et al. (2001). Data for the updraft and downdraft mass fluxes, however, are not available for some SCMs.

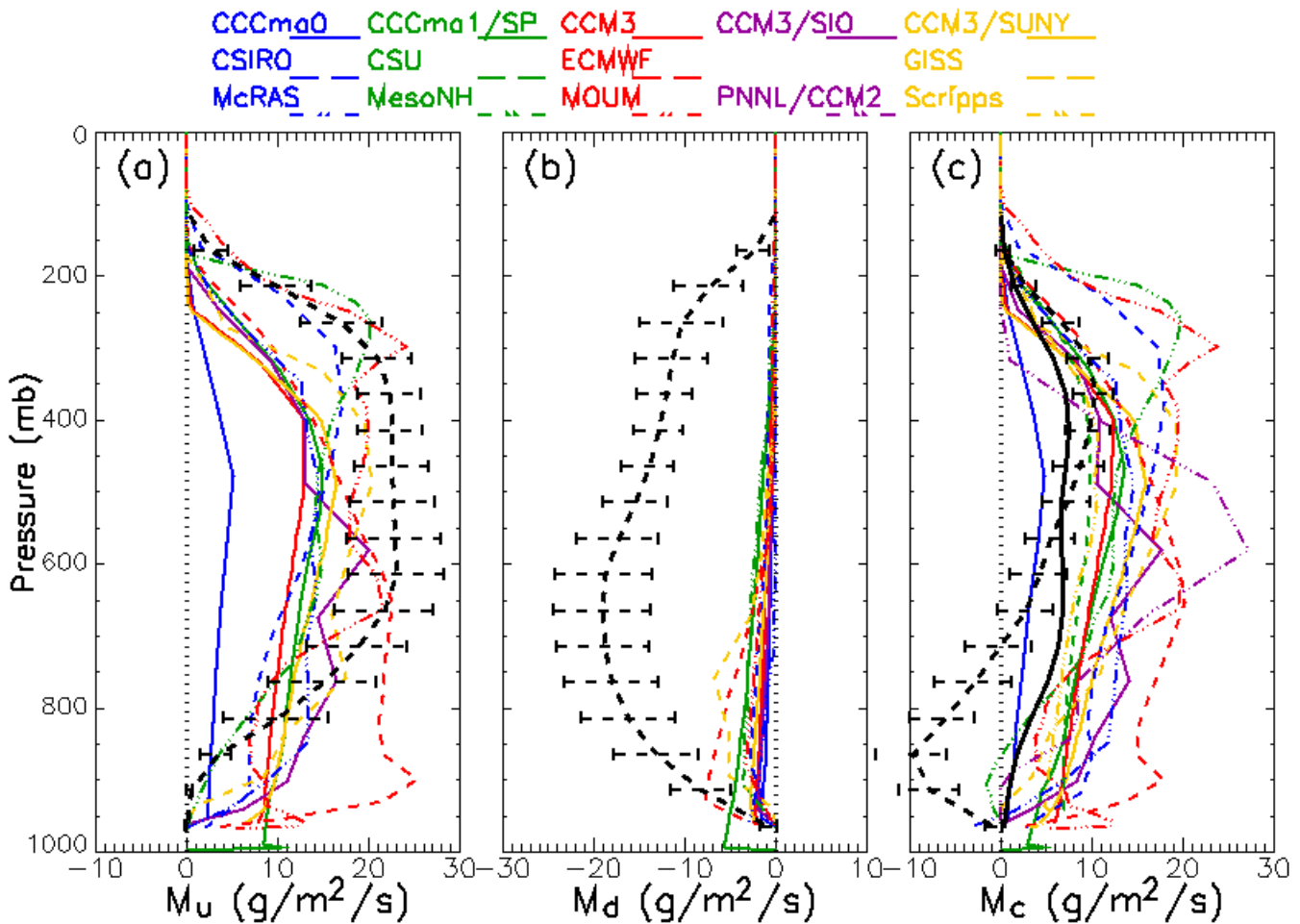


Figure 5. Vertical profiles of (a) updraft, (b) downdraft, and (c) net cumulus mass fluxes averaged over the disturbed periods (observed precipitation rates $> 0.36 \text{ mm day}^{-1}$) during Subcases A, B, and C. Black solid line is the observed large-scale mean mass flux ($-\omega$). Black dashed line and small bar represent the mean of the mass fluxes across the 10 CRMs and the standard deviations from the mean, respectively.

The CRM's large M_u is seen in the middle and upper troposphere between 300 to 700 hPa. Downdraft mass flux M_d has comparable magnitude with M_u in the CRMs. The maximum M_d is around 600 hPa. As a result, the net mass flux M_c is relatively small compared to the updraft and downdraft mass fluxes. It is positive in the middle and upper troposphere and negative in the lower troposphere. As shown in Raymond (1993), this is a typical vertical structure of the net cloud mass fluxes in cumulonimbus clouds in mid-latitudes where cloud base heights and PBL depths are usually higher and the precipitation-induced downdrafts can equal or exceed updrafts in the lower parts of cumulonimbi.

Compared to the CRMs, the updraft mass flux in the SCMs is smaller in the middle and upper troposphere and larger in the lower troposphere. The vertical extension of the updrafts in the upper troposphere is smaller in most SCMs except for CSIRO, MesoNH, and MOUM. The downdrafts in the

SCMs are very weak. This leads to larger net mass fluxes in the SCMs, especially in the lower troposphere. Most models fail to produce the negative mass flux shown in the CRMs because of the weak downdrafts. Only MesoNH exhibits small negative mass flux in the lower troposphere.

It should be noted that there are differences in defining cloud mass fluxes between CRMs and SCMs. In the CRMs, the cloud mass fluxes contain all types of updrafts and downdrafts including convective-scale and mesoscale updrafts and downdrafts. In contrast, the SCMs only parameterize convective-scale updrafts and convective-scale precipitation-induced downdrafts. The neglect of mesoscale circulation in the SCMs is at least partly responsible for the large discrepancies between the CRMs and SCMs. Many studies have shown that mass fluxes in mesoscale updrafts and downdrafts are significant relative to convective mass fluxes.

To quantify the importance of mesoscale circulations, results from UCLA/CSU CRM are further analyzed. Figure 6 compares the mass fluxes in convective-scale and mesoscale regions. The mass fluxes are averaged over the same disturbed periods as those in Figure 5. In the figure, solid lines represent total mass fluxes, dotted lines represent convective-scale contributions, and dashed lines are mesoscale contributions. The partitioning method used for this analysis is described in Xu (1995).

Figure 6 (a) shows that the convective-scale updraft is a major contributor to the total updraft mass flux at levels below 300 hPa. The maximum convective-scale updraft appears in the middle troposphere (around 600 hPa) while the maximum mesoscale updraft appears in the upper troposphere (around

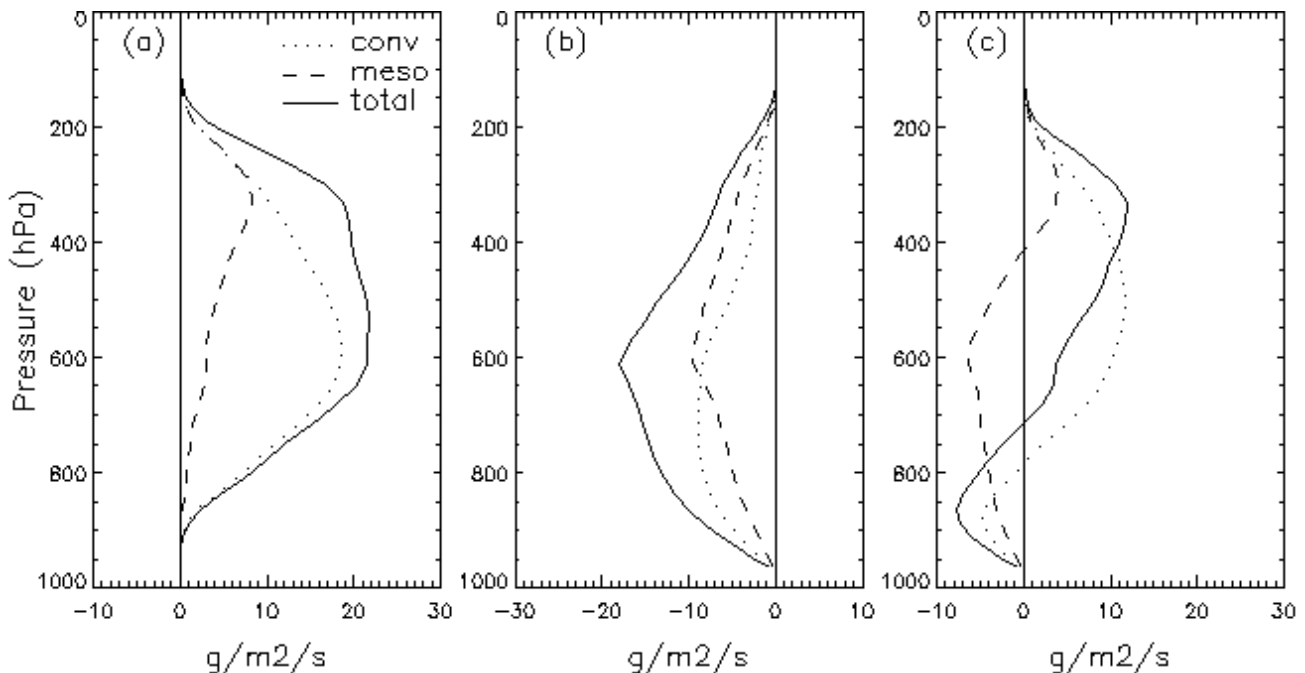


Figure 6. Vertical profiles of (a) updraft, (b) downdraft, and (c) net cumulus mass fluxes estimated from UCLA/CSU CRM averaged over the disturbed periods (observed precipitation rates $> 0.36 \text{ mm day}^{-1}$) during Subcases A, B, and C. Solid lines represent the total mass fluxes, dashed lines convective-scale contributions, and dotted lines mesoscale contributions.

300 hPa). In contrast to the updrafts, the mesoscale downdrafts have comparable values with the convective-scale downdrafts. The mesoscale downdrafts are larger than the convective-scale downdrafts above 600 hPa and smaller below. The convective-scale downdrafts are mainly located in the lower part of the troposphere. For the net mass fluxes, the convective-scale mass flux is dominated by the convective-scale updrafts throughout whole troposphere except for the levels below 800 hPa, while the mesoscale mass flux is dominated by the mesoscale downdrafts in the middle and lower troposphere. As is seen from Figure 5, the SCMs generally capture well the convective-scale updrafts but most of the SCMs still significantly underestimate the convective-scale downdrafts except for GISS and ECMWF, indicating possible problems with the parameterizations of convective-scale downdrafts. Because mass fluxes diagnosed from CRMs have noticeable intermodel differences, we caution that it is not possible to draw firm conclusions based on results from one CRM. The partitioning of results from other CRMs need to be investigated.

It should be noted that large uncertainties remain in the mass flux diagnosed from the CRMs and the methodology used for partitioning the total mass flux into convective-scale and mesoscale components. This can be another reason for the large discrepancies between the SCMs and the CRMs. For example, Xu et al. (2001) showed that the diagnosed mass fluxes in the CRMs include contributions not only from convective-scale and mesoscale circulations, but also from gravity waves because many different scales of motions are present in CRM simulations. Therefore, some of the strong updrafts and downdrafts in the upper troposphere are related to unrealistically strong gravity wave activities in the simulations. An analysis method for eliminating gravity wave contributions to the updrafts and downdrafts is highly desired.

Conclusions

We conclude that:

1. The SCM simulation errors are closely related to problems with model cumulus parameterizations. The schemes with triggering based on CAPE generally produce more active cumulus convection than the schemes with triggering based on local parcel buoyancy over land surface at mid-latitudes because CAPE is usually large and is mainly determined by the strong solar diurnal heating there. The use of positive CAPE to trigger model convection can lead to an overestimation of convection during the daytime. This results in warmer/drier atmospheres in the former and cooler/moister atmospheres in the latter.
2. A non-penetrative convection scheme can underestimate the depth of conditional instability for deep mid-latitude continental convection, and therefore results in a cooler atmosphere in the upper troposphere.
3. The updraft mass fluxes in the SCMs agree quantitatively well with those in the CRMs. In contrast, most SCMs produce very weak downdraft mass fluxes compared to those diagnosed from the CRMs. These discrepancies are primarily attributable to the neglect of mesoscale circulations in the SCMs, uncertainties in the diagnosed mass fluxes from the CRMs, and deficiencies in the SCM parameterizations of mass fluxes.

Corresponding Author

Dr. Shaocheng Xie, xie2@llnl.gov, (925) 422-6023

References

Arakawa, A., and W. H. Schubert, 1974: Interaction of a cumulus cloud ensemble with the large-scale environment, Part I. *J. Atmos. Sci.*, **31**, 674-701.

Ghan, S. J., R. T. Cederwall, D. Cripe, J. Hack, S. Iacobellis, S. Klein, S. Krueger, V. Lohmann, J. Pedretti, D. Randall, A. Robock, L. Rolstain, R. Somerville, G. Stenchikoo, J. Sud, G. Walker, S. C. Zie, K.-M. Xu, J. J. Yio, and M. Zhang, 2000: An intercomparison of single column model simulations of summertime mid-latitude continental convection. *J. Geophys. Res.*, **105**, 2091-2124.

Raymond D. J., 1993: Observational constraints on cumulus parameterization in *The Representation of Cumulus Convection in Numerical Models*, Meteorol. Monogr., eds. K. Emanuel and D. Raymond, **46**, p. 246, Amer. Meteorol. Soc., Boston, Massachusetts.

Xie, S. C., and M. H. Zhang, 2000: Impact of the convective triggering function on single-column model simulations. *J. Geophys. Res.*, **105**, 14,983-14,996.

Xie, S. C., R. T. Cederwall, J. J. Yio, and K.-M. Xu, 2001: Intercomparison and evaluation of cumulus parameterizations under summertime mid-latitude continental conditions. *Q. J. R. Meteorol. Soc.*, submitted.

Xu, K.-M., 1995: Partitioning mass, heat and moisture budgets of explicitly simulated cumulus ensembles into convective and stratiform components. *J. Atmos. Sci.*, **52**, 551-573.

Xu, K.-M., et al., 2001: An intercomparison of cloud-resolving models with the ARM summer 1997 IOP data. *Q. J. R. Meteorol. Soc.*, submitted.

Zhang, G. J., and N. A. McFarlane, 1995: Sensitivity of climate simulations to the parameterization of cumulus convection in the Canadian Climate Center general circulation model. *Atmosphere-Ocean*, **33**, 407-446.

Zhang, M. H., and J. L. Lin, 1997: Constrained variational analysis of sounding data bases on column-integrated budgets of mass, heat, moisture, and momentum: Approach and application to ARM measurements. *J. Atmos. Sci.*, **54**, 1503-1524.

Zhang, M. H., J. L. Lin, R. T. Cederwall, J. J. Yio, and S. C. Xie, 2001: Objective analysis of ARM IOP Data: Method and sensitivity. *Mon. Weather Rev.*, **129**, 295-311.